

# Towards Lifelong Self-Supervision For Unpaired Image-to-Image Translation

Victor Schmidt\*, Makesh Narsimhan Sreedhar, Mostafa ElAraby, Irina Rish

Mila  
Universite de Montreal

## Abstract

*Unpaired Image-to-Image Translation (I2IT) tasks often suffer from lack of data, a problem which self-supervised learning (SSL) has recently been very popular and successful at tackling. Leveraging auxiliary tasks such as rotation prediction or generative colorization, SSL can produce better and more robust representations in a low data regime. Training such tasks along an I2IT task is however computationally intractable as model size and the number of task grow. On the other hand, learning sequentially could incur catastrophic forgetting of previously learned tasks. To alleviate this, we introduce Lifelong Self-Supervision (LiSS) as a way to pre-train an I2IT model (e.g., CycleGAN) on a set of self-supervised auxiliary tasks. By keeping an exponential moving average of past encoders and distilling the accumulated knowledge, we are able to maintain the networks validation performance on a number of tasks without any form of replay, parameter isolation or retraining techniques typically used in continual learning. We show that models trained with LiSS perform better on past tasks, while also being more robust than the CycleGAN baseline to color bias and entity entanglement (when two entities are very close).*

## 1. Introduction

### 1.1. Motivation

In recent years generative unsupervised image-to-image translation (I2IT) has gained tremendous popularity, enabling style transfer [43] and domain adaptation [10], raising awareness about wars [40] and Climate Change [37] and even helping model cloud reflectance fields [38]. I2IT has become a classical problem in computer vision which involves learning a conditional generative mapping from a

source domain  $\mathcal{X}$  to a target domain  $\mathcal{Y}$ . For example, generating an image  $\hat{y}$  of a zebra conditioned on an image  $x$  of a horse. Obviously, there is no ground-truth data for this transformation and we cannot therefore leverage pairs  $(x, y)$  to learn this generative mapping. This is the challenge that unpaired I2IT addresses.

One of the main limitations of the I2IT task is that data is often scarce and hard to acquire [24, 37, 43]. To overcome this difficulty, self-supervised learning (SSL) appears to be a promising approach. In SSL, a model is trained on an *auxiliary task* (e.g., image rotations prediction) that leverages unsupervised data in order to obtain better representations which can help a downstream task learn faster when few (labeled) samples are available [17]. Given the variety of such potential auxiliary tasks, one could hope to jointly train many of them along with the main task, thereby improving the performance on the latter. However, this may be impractical in the context of I2IT since the models are typically quite large, making parallel training of self-supervised and translation tasks computationally intractable. On the other hand, any form of sequential learning may result into catastrophic forgetting [5] and counter the benefits of SSL. In this paper, we therefore investigate how *continual learning*, a set of approaches designed to make sequential learning across multiple tasks robust to catastrophic forgetting, can be used to enable self-supervised pre-training of unpaired I2IT models.

We show that self-supervised auxiliary tasks improve CycleGAN’s translations with more semantic representations and that distillation [9, 42] retains the knowledge acquired while pre-training the networks. For easier reference, we call this framework ”Lifelong Self-Supervision”, or *LiSS*, and show its results on CycleGAN’s performance in Section 3.

### 1.2. Related Work

Generative Adversarial Networks (GANs) [7] have had tremendous success in generating realistic and diverse images [1, 19, 41]. Generative I2IT approaches often

\*For correspondence: schmidtv@mila.quebec  
Work under review for CVPR 2020’s Continual Vision Workshop.  
Code: <https://github.com/vict0rsch/LiSS>

leverage GANs to align the distributions of the source and target domains and produce realistic translations [12]. In their seminal work, Isola et al. [14] proposed a principled framework for I2IT by introducing a weighted average of a conditional GAN loss, along with an  $L_1$  reconstruction loss to leverage pairs (for instance edges  $\leftrightarrow$  photos or labels  $\leftrightarrow$  facade). To address the setting where pairs are not available, Zhu et al. [43] introduced the cycle-consistency loss which uses two networks to symmetrically model source $\rightarrow$ target and source $\leftarrow$ target. The cycle-consistency induces a type of self-supervision by enforcing a reconstruction loss when an image goes through one network and then the other. Many attempts have since been made to improve the diversity [12, 24] and semantic consistency [31, 32] of CycleGAN-inspired I2IT models by leveraging an encoder-decoder view of the models. We keep with the CycleGAN encoder-decoder model, and use self-supervision to encourage the encoder to encode meaningful features for the decoder to work with (see section 2 for more details).

Self-supervised learning tries to leverage the information already present in samples to produce data-efficient representations. This is often measured by pre-training a standard supervised network on an auxiliary (or *pretext*) task, and then measuring its performance on the actual dataset on a fixed, low budget of labels [17]. Though not new [2], it has gained a lot of popularity in the deep learning era with important successes in language modeling [3, 11, 34] speech recognition [36], medical imaging [35] and computer vision in general [17]. Indeed, computer vision models seem to benefit significantly from self-supervised learning as the amount of unlabeled data can be very large, while labeling can be expensive [17]. In this context, many visual pre-training tasks have been proposed, such as image rotation prediction [6], colorization [13], and solving jigsaw puzzles [33]. In addition to these context-based and generation-based pre-training methods, one can also leverage pseudo-labels from a pre-trained model in free semantic label-based methods [17]. In our work we therefore add a depth prediction pretext task, as advocated by [4], based on inferences from MegaDepth [26]. As the number of pretext tasks increases, so does the memory and computational time needed to process samples. This is especially problematic for generation-based methods which can be as computationally and memory intensive as the downstream task’s model. We cannot therefore hope to train large models such as those used in I2IT, in parallel with all these tasks.

One must therefore derive a learning procedure which ensures that the networks do not forget as they change tasks: this is the focus of continual (or lifelong) learning. Neural networks have been plagued by the inability to main-

tain performance on previously accomplished tasks when they are trained on new ones - a phenomenon that has been coined *catastrophic forgetting* [20]. Various continual learning methods have been developed to mitigate forgetting which can be categorized as follows [21]: replay-based methods, regularization-based methods and parameter isolation methods. In their work, Matsumoto and Yanai [30] use the parameter-isolation method PiggyBack [29] in order to learn a sequence of I2IT tasks without forgetting the previous ones. Zhai et al. [42] on the other hand uses distillation [9] in order to perform such tasks. In this work, we borrow ideas from the latter and apply them to a sequence of self-supervised tasks followed by a translation task.

## 2. Approach

### 2.1. Model

Our main contribution is a continual learning framework which maintains self-supervised performance and improves unpaired I2IT representations. We chose as our I2IT model the simple and well-understood CycleGAN [43].

Let  $\mathcal{T}$  be a set of  $n = |\mathcal{T}|$  tasks such that  $\{T^{(k)} | k < n - 1\}$  is a set of self-supervised tasks and  $T^{(n-1)}$  is an I2IT task such as horse $\leftrightarrow$ zebra [43]. The model is composed of two domain-specific sets of networks  $M_A = \{G_A, D_A\}$  and  $M_B = \{G_B, D_B\}$  where  $G_i$  is a multi-headed generator and  $D_i$  is a set of discriminators (1 per generative pretext task and 1 for the translation task). From now on,  $i$  will be either  $A$  or  $B$  in which case  $j$  is  $B$  or  $A$ . All the following is symmetric in  $i$  and  $j$ .

Let us focus on  $G_i$ . It is composed of an encoder  $E_i$  and a set of  $n$  task-specific heads  $H_i^{(k)}$  which map from the encoder’s output space to  $T^{(k)}$ ’s output space. Let  $x_i$  be a sample from domain  $i$  and  $z_i = E_i(x_i)$ . In our work, we focus on the following 4 pretext tasks:

1.  $T^{(0)}$  is a rotation task, inspired from [6], and  $H_i^{(0)}$  performs a classification task:  $H_i^{(0)}(z_i) \in [0, 1]^4$  as there are 4 possible rotations ( $0^\circ$ ,  $90^\circ$ ,  $180^\circ$  and  $270^\circ$ ). When appropriate (see 2.2) we train  $H_i^{(0)} \circ E_i$  with a cross-entropy objective  $\mathcal{L}^{(0)}$ .
2.  $T^{(1)}$  is a jigsaw puzzle as introduced by [33]. We split the image into 9 equal sub-regions which we randomly reorder according to 64 pre-selected permutations (out of the  $9!$  possible ones):  $H_i^{(1)}(z_i) \in [0, 1]^{64}$ . Similarly, we train  $H_i^{(1)} \circ E_i$  with a cross-entropy objective  $\mathcal{L}^{(1)}$ .
3.  $T^{(2)}$  is a relative depth prediction task inspired from [16]:  $H_i^{(2)}(z_i) \in \mathbb{R}^{h \times w}$ .  $H_i^{(2)} \circ E_i$  is trained with an  $L_1$  objective  $\mathcal{L}^{(2)}$  with respect to pseudo-labels obtained from a pre-trained MegaDepth model [26].

4.  $T^{(3)}$  is a colorization task, as per [13, 22]:  $H^{(3)}(z_i) \in [-1, 1]^{3 \times h \times w}$ . Because a gray image can have several possible colorizations, we train  $H_i^{(3)} \circ E_i$  by a mixture of  $L^1$  loss with respect to  $x_i$  and a GAN loss from a discriminator  $D_i^{(3)}$ :  $\mathcal{L}^{(3)} = 0.1L_1 + 0.9L_{GAN}$

The downstream translation task is based on CycleGAN’s losses. For simplicity, in the following equations we call  $G_i$  what is actually  $H_i^{(4)} \circ E_i$ , that is to say the standard CycleGAN generator.

$$L_{GAN} : (G_i, D_i, x_i, x_j) \mapsto \mathbb{E}_{x_i} [\log(D_i(x_i))] + \mathbb{E}_{x_j} [\log(1 - D_i(G_i(x_j)))] \quad (1)$$

$$L_{idt} : (G_i, x_i) \mapsto \|x_i - G_i(x_i)\|_1 \quad (2)$$

$$L_{cyc} : (G_i, G_j, x_i) \mapsto \|x_i - G_i(G_j(x_i))\|_1 \quad (3)$$

$$\mathcal{L}^{(4)} = L_{GAN} + \lambda_{idt}L_{idt} + \lambda_{cyc}L_{cyc} \quad (4)$$

The overall model for domain  $i$  is therefore composed of a shared encoder network and a set of  $n$  heads which map from this latent space to their specific task’s output space. We now need to understand how these tasks can be combined together in order to enable forward transfer from each of the self-supervised tasks to the translation task, without forgetting.

## 2.2. Training Schedule

When trying to incorporate self-supervised learning ideas into the I2IT framework, one could naively train all the heads in *parallel* ( $\lambda^{(k)}$  are scalars weighting the contribution of each loss):

$$\mathcal{L}^{parallel} = \sum_{k=0}^{n-1} \lambda^{(k)} \mathcal{L}^{(k)} \quad (5)$$

As explained previously, not only is this approach slower in that each sample has to go through all heads, but it also forces us to use smaller batch sizes for memory constraints.

Another naive approach would be to perform each task sequentially. Given an ordering  $\tau$  of  $\mathcal{T}$ , one could train the model with:

$$\mathcal{L}_{\tau^{(k)}}^{sequential} = \lambda^{(\tau(k))} \mathcal{L}^{(\tau(k))} \quad (6)$$

In this *sequential* training schedule, the model transitions from  $(H_i^{(k)}, \mathcal{L}_k^{sequential})$  to  $(H_i^{(k+1)}, \mathcal{L}_{k+1}^{sequential})$  according to some curriculum. For readability and without loss of generality, we omit  $\tau$  from now on. In our experiments we implement a threshold-based curriculum where the transition from one task to the next depends on its performance (in both domains  $A$  and  $B$ ) on some validation metric (see Section 3.1).

In this paper we introduce Lifelong Self-Supervision, a *continual* schedule which is similar to the sequential with the addition of a distillation loss. Inspired by Tarvainen and Valpola [39], we maintain an exponential moving average of past encoder parameters, therefore keeping a weighted memory of all past encoders at the cost of single additional one. Formally, let  $E_i^{(k)}$  be the frozen state of  $E_i$  at the end of the  $k^{th}$  task, *i.e.* when transitioning from  $T^{(k)}$  to  $T^{(k+1)}$ . Then we define the (non-trainable) reference encoder  $\tilde{E}_i^{(k)}$  as follows:

$$\tilde{E}_i^{(k)} = \begin{cases} 0 & \text{if } k = 0 \\ E_i^{(0)} & \text{if } k = 1 \\ \alpha E_i^{(k-1)} + (1 - \alpha) \tilde{E}_i^{(k-1)} & \text{if } k > 1 \end{cases} \quad (7)$$

With  $\alpha \in [0, 1]$ . We use  $\tilde{E}_i$  in an additional distillation term in the loss, minimizing the distance between the current and reference encoded spaces:

$$L_{dist}^{(k)} : (\tilde{E}_i^{(k)}, E_i, x_i) \mapsto \|\tilde{E}_i^{(k)}(x_i) - E_i(x_i)\|_1 \quad (8)$$

$$\mathcal{L}_t^{continual} = \mathcal{L}_t^{sequential} + \beta L_{dist}^{(t)} \quad (9)$$

These ideas are general and not specific to I2IT or CycleGAN ; this is why LiSS refers to  $(\mathcal{T}, \mathcal{L}^{continual})$ , not to a specific model.

## 3. Experiments

### 3.1. Setup

To evaluate the effect of LiSS on CycleGAN’s performance, we compare it with a baseline CycleGAN from [43] and to the two aforementioned naive training schedules: *sequential* and *parallel*. We compare these 4 models on the horse $\leftrightarrow$ zebra dataset on a dataset of flooded $\leftrightarrow$ non-flooded street-level scenes from [37] (the task is to simulate floods). As our goal is to understand how to efficiently leverage a set of given pretext tasks to improve representations, we keep  $\mathcal{T}$  constant across experiments.

All models are trained with the same hyper-parameters. We use the RAdam optimizer [27] with a learning rate of 0.0005. We keep  $\lambda_{idt}$  and  $\lambda_{cyc}$  to their default values and set all  $\lambda^{(k)}$  to 1. We leave the analysis of  $\alpha$ ’s exact impact for future work and set it to 0.5 across experiments (see Eq. 7). Results are compared after 230k translation steps. The continual and sequential models therefore have more total steps of training but in all cases  $H_i^{(n-1)}$  is trained for 230k steps (*i.e.* 24 hours of training with the LiSS training schedule). We set a fixed curriculum as per section 2.1 with thresholds at 85% for classification tasks, and  $L_1$  distance

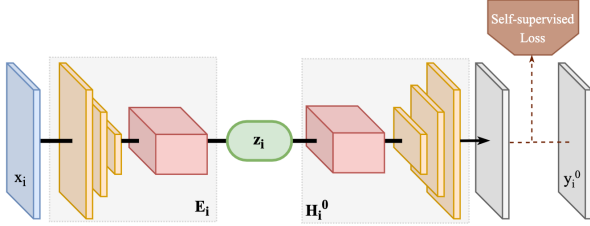


Figure 1: Training of the first pretext task  $H_i^{(0)} \circ E_i$ . Orange blocks are (de-)convolutions, red blocks are sets of residual blocks. Here,  $H_i^{(0)}$ 's structure is for illustration purposes, see Appendix A for more details

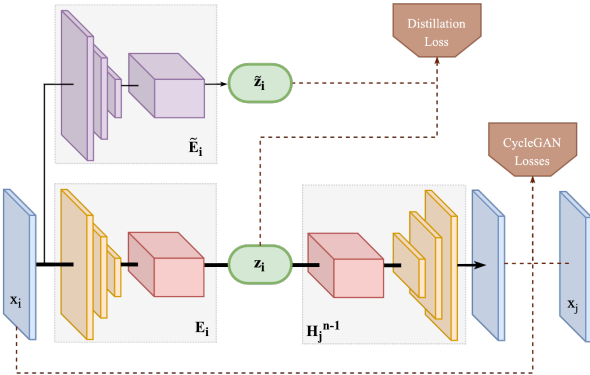


Figure 2: Training of the translation task  $H_j^{(n-1)} \circ E_i$ . As all tasks  $T^{(k>0)}$ , it includes a distillation loss between the current encoder's output  $z$  and the reference encoder's,  $z^{ref}$ .

of 0.15 for regression tasks. These were set to be  $\sim 95\%$  of the parallel schedule's final validation performance. Batch-size is set to 5, for LiSS and *sequential* schedules, but to 3 for the *parallel* schedule<sup>1</sup>.

### 3.2. Image-to-Image Translation

Figure 3 and 4 show how the LiSS framework visually fares against the other schedules. Images are referred to as  $[i, j]$  meaning row  $i$  and column  $j$  in those figures.

While our setup does not quite match the pixelwise translation performance of CycleGAN, the model learns some interesting semantic features. Unlike CycleGAN which tends to merge distinct instances of entities that are very close to each other (Figure 3's image  $[1, 1]$  for instance), our model is able to disentangle these instances and retain them as separate entities after translation. We can also see from Figure 3's image  $[1, 4]$  and Figure 4's images  $[1, 0]$  and  $[1, 2]$  that CycleGAN relies on color-based features, as evidenced by the zebra stripes projected on the brown patch of ground and the sky artifacts. On the other hand,

<sup>1</sup>these are the largest values which fit in a Nvidia V100's 16GB of GPU memory.

adding self-supervised tasks makes the models less sensitive to such glaring errors (see rows below the aforementioned CycleGAN translations in Figures 3 and 4).

Compared to the parallel schedule, LiSS keeps relevant features without enforcing a continuous training of  $H_i^{(k<n-1)}$ , which gives useful freedom to the model. It is able to have a similar translation performance and better color consistency, though one could argue that the parallel's translations are visually slightly better.

The sequential schedule on the other hand seems to have slightly worse translation performance. We can see that some of the useful "knowledge" the two other models still have is no longer available to the translation head as the smaller zebra is merged with the taller one in Figure 3's image  $[4, 1]$  and the brown patch in image  $[4, 4]$  shows slight stripes.

### 3.3. Continual Learning Performance

Our main finding is that Lifelong Self-Supervision partially prevents forgetting. We can see in figures 5 and 6 that our formulation preserves the model from a forgetting as severe as in *sequential* training while providing enough flexibility for it to learn new tasks.

In both datasets, we observe that the naive training schedules behave as expected: the *sequential* one is able to learn new tasks the fastest as the model is less constrained. However, it is noticed that the sequential setup forgets previous tasks almost instantly as it changes its focus to a new task. On the other hand, the more constrained *parallel* schedule shows that continuously training on tasks allows the model to master them all at once. This however comes at a memory and time cost as we could not fit more than 3 samples per batch (vs 5 for the other schedules), and the average processing time per sample is much larger (0.27s against an average of 0.12s for the other schedules). This means that to complete 230k translation steps, the *parallel* schedule typically takes more than 17h when LiSS only takes 12h (counting all the pretext tasks).

Figures 5 and 6 show how LiSS maintains accuracies for the Rotation and Jigsaw tasks while performing slightly worse on the Depth prediction and Colorization tasks. As the encoder produces increasingly richer representations, the distillation loss prevents it from mapping input images to regions that would harm previous tasks. Because of our problem's sequential nature, decoding heads  $H_i^{(k<n-1)}$  do not change after they have achieved the curriculum's required performance and the burden of producing stable yet informative features entirely relies on the encoders  $E_i$  as the heads cannot adjust to its changes.

Table 1 and 2 show that it takes more steps for the tasks to be learnt with LiSS. Intuitively, when training sequen-



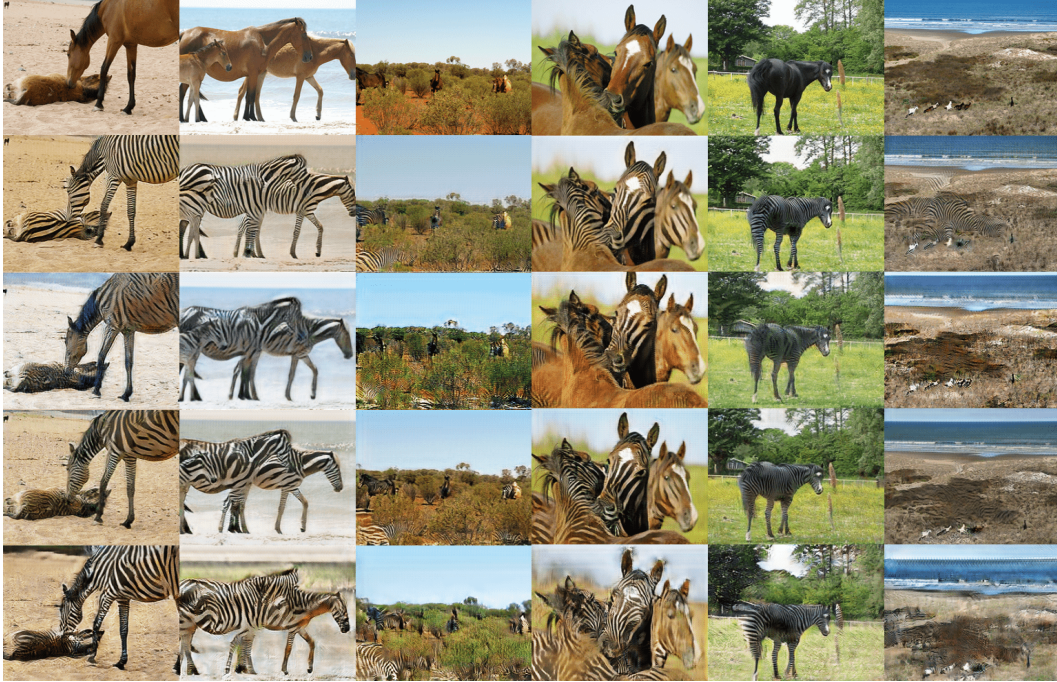


Figure 3: Comparison of models on the horse $\leftrightarrow$ zebra dataset, with rows corresponding the image to translate (row 0) then translations from: CycleGAN (row 1), LiSS CycleGAN (row 2), Parallel Schedule (row 3), Sequential schedule(row 4). Note: the slight discrepancy in cropping is due to data-loading randomness



Figure 4: Comparison of models on the flooded $\leftrightarrow$ non-flooded dataset, with rows corresponding the image to translate (row 0) then translations from: CycleGAN (row 1), LiSS training (row 2), parallel training (row 3), sequential training (row 4).

tially, the encoders are free to adjust exactly to the task. When training with LiSS, they are more constrained and it takes more iterations for them to reach the same performance on pretext tasks. This constraint is however pliable enough for encoders to adjust to new tasks.

Schedule	Task	Start_Step	End_Step
LiSS	Rotation	0	8 000
	Jigsaw	8 000	158 000
	Depth	158 000	170 000
	Colorization	170 000	172 000
Sequential	Rotation	0	24 000
	Jigsaw	24 000	96 000
	Depth	96 000	102 000
	Colorization	102 000	108 000

Table 1: Transition steps for the horse↔zebra task. Transition starts when the colorization task is mastered.

#### 4. Discussion

We propose a method, Lifelong Self-Supervision (LiSS), enabling CycleGAN to leverage sequential self-supervised auxiliary tasks to improve its representations. By distilling the knowledge of a reference encoder (which is an exponential moving average of previous encoders, in parameter space) we prevent catastrophic forgetting of the auxiliary tasks, thereby allowing CycleGAN to better disentangle instances of objects to be translated and rely less on colors. This framework can bring benefits of training on all the tasks at once at a much lower memory and computational cost as it only requires us to keep one additional encoder. Our exploratory experiments show encouraging results which will need further investigation in future work to produce a principled framework.

Open questions include the exact impact of the reference encoder’s algebra (namely exponential moving average versus other moving averages and the impact of  $\alpha$ ), a more thorough hyper-parameter search in order to tune  $\lambda^{(k)}$  and  $\beta$  and achieve better pixel-level results. Additionally, exploring schedules and auxiliary tasks would allow for a better understanding of how SSL can improve unpaired I2IT models. Finally, while CycleGAN’s simplicity allowed us to isolate LiSS’s contribution to improved translations, exploring its capabilities on more complex architecture is a promising direction for future work.

#### References

- [1] A. Brock, J. Donahue, and K. Simonyan. Large scale gan training for high fidelity natural image synthesis. *arXiv preprint arXiv:1809.11096*, 2018.
- [2] V. R. de Sa. Learning classification with unlabeled data. In *Advances in neural information processing systems*, pages 112–119, 1994.
- [3] J. Devlin, M.-W. Chang, K. Lee, and K. Toutanova. Bert: Pre-training of deep bidirectional transformers for language understanding. *arXiv preprint arXiv:1810.04805*, 2018.
- [4] C. Doersch and A. Zisserman. Multi-task self-supervised visual learning. *arXiv preprint arXiv:1708.07860*, 2017.
- [5] R. M. French. Catastrophic forgetting in connectionist networks. *Trends in Cognitive Sciences*, 3(4):128 – 135, 1999. ISSN 1364-6613. doi: [https://doi.org/10.1016/S1364-6613\(99\)01294-2](https://doi.org/10.1016/S1364-6613(99)01294-2). URL <http://www.sciencedirect.com/science/article/pii/S1364661399012942>.
- [6] S. Gidaris, P. Singh, and N. Komodakis. Unsupervised representation learning by predicting image rotations. *arXiv preprint arXiv:1803.07728*, 2018.
- [7] I. Goodfellow, J. Pouget-Abadie, M. Mirza, B. Xu, D. Warde-Farley, S. Ozair, A. Courville, and Y. Bengio. Generative adversarial nets. In Z. Ghahramani, M. Welling, C. Cortes, N. D. Lawrence, and K. Q. Weinberger, editors, *Advances in Neural Information Processing Systems 27*, pages 2672–2680. Curran Associates, Inc., 2014. URL <http://papers.nips.cc/paper/5423-generative-adversarial-nets.pdf>.
- [8] K. He, X. Zhang, S. Ren, and J. Sun. Deep residual learning for image recognition. In *Proceedings of the IEEE conference on computer vision and pattern recognition*, pages 770–778, 2016.
- [9] G. Hinton, O. Vinyals, and J. Dean. Distilling the knowledge in a neural network. *arXiv preprint arXiv:1503.02531*, 2015.
- [10] J. Hoffman, E. Tzeng, T. Park, J.-Y. Zhu, P. Isola, K. Saenko, A. A. Efros, and T. Darrell. Cycada: Cycle-consistent adversarial domain adaptation. *arXiv preprint arXiv:1711.03213*, 2017.
- [11] J. Howard and S. Ruder. Universal language model fine-tuning for text classification. *arXiv preprint arXiv:1801.06146*, 2018.
- [12] X. Huang, M.-Y. Liu, S. Belongie, and J. Kautz. Multimodal unsupervised image-to-image translation. *arXiv preprint arXiv:1804.04732*, 2018.
- [13] S. Iizuka, E. Simo-Serra, and H. Ishikawa. Let there be color! joint end-to-end learning of global and local image priors for automatic image colorization with simultaneous classification. *ACM Transactions on Graphics (ToG)*, 35(4):1–11, 2016.
- [14] P. Isola, J.-Y. Zhu, T. Zhou, and A. A. Efros. Image-to-image translation with conditional adversarial networks. *arXiv preprint arXiv:1611.07004*, 2016.
- [15] P. Isola, J.-Y. Zhu, T. Zhou, and A. A. Efros. Image-to-image translation with conditional adversarial networks. In *Proceedings of the IEEE conference on computer vision and pattern recognition*, pages 1125–1134, 2017.

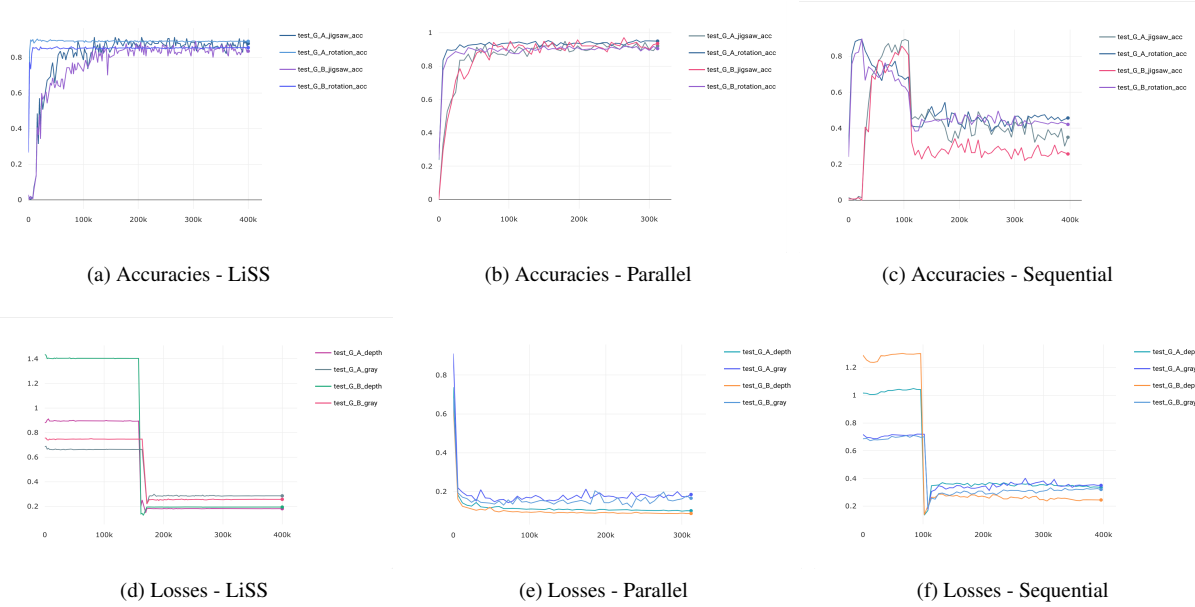


Figure 5: Validation performance of the various schedules on the **horse↔zebra** dataset. Accuracies are reported in the top row for the rotation and jigsaw heads of both  $G_A$  and  $G_B$ . Similarly, colorization (named *gray* in the plots) and depth prediction regression performances are plotted in the bottom row. Note how, unlike *sequential* training, LiSS training maintains validation accuracies even though the model does not see the tasks anymore. Losses bump a little but converge to a better value than the sequential’s. This illustrates how the LiSS training framework enables the model to leverage independent tasks’ benefits while maintaining sufficient flexibility to learn new tasks, at a very low cost.

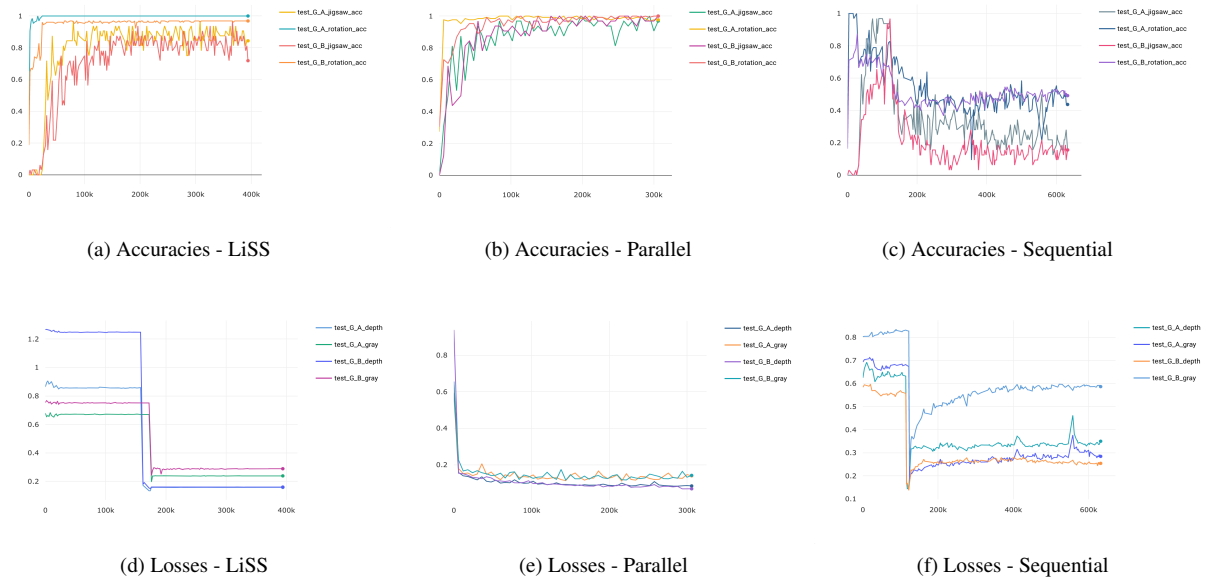


Figure 6: Same plots as in Figure 6 for the **flooded↔non-flooded** dataset. Once again we can see the drastic difference between LiSS and the naive *sequential* training schedule. The difference is much milder when comparing LiSS with *parallel* training. The distillation loss prevents forgetting and maintains performance while allowing the network to learn new tasks. Transition steps are referenced in the Appendix’s table 2.



- [16] H. Jiang, E. Learned-Miller, G. Larsson, M. Maire, and G. Shakhnarovich. Self-supervised relative depth learning for urban scene understanding. *arXiv preprint arXiv:1712.04850*, 2017.
- [17] L. Jing and Y. Tian. Self-supervised visual feature learning with deep neural networks: A survey. *arXiv preprint arXiv:1902.06162*, 2019.
- [18] J. Johnson, A. Alahi, and L. Fei-Fei. Perceptual losses for real-time style transfer and super-resolution. In *European conference on computer vision*, pages 694–711. Springer, 2016.
- [19] T. Karras, S. Laine, M. Aittala, J. Hellsten, J. Lehtinen, and T. Aila. Analyzing and improving the image quality of stylegan. *arXiv preprint arXiv:1912.04958*, 2019.
- [20] J. Kirkpatrick, R. Pascanu, N. Rabinowitz, J. Veness, G. Desjardins, A. A. Rusu, K. Milan, J. Quan, T. Ramalho, A. Grabska-Barwinska, et al. Overcoming catastrophic forgetting in neural networks. *Proceedings of the national academy of sciences*, 114(13):3521–3526, 2017.
- [21] M. D. Lange, R. Aljundi, M. Masana, S. Parisot, X. Jia, A. Leonardis, G. Slabaugh, and T. Tuytelaars. Continual learning: A comparative study on how to defy forgetting in classification tasks. *arXiv preprint arXiv:1909.08383*, 2019.
- [22] G. Larsson, M. Maire, and G. Shakhnarovich. Colorization as a proxy task for visual understanding. In *CVPR*, 2017.
- [23] C. Ledig, L. Theis, F. Huszár, J. Caballero, A. Cunningham, A. Acosta, A. Aitken, A. Tejani, J. Totz, Z. Wang, et al. Photo-realistic single image super-resolution using a generative adversarial network. In *Proceedings of the IEEE conference on computer vision and pattern recognition*, pages 4681–4690, 2017.
- [24] H.-Y. Lee, H.-Y. Tseng, J.-B. Huang, M. Singh, and M.-H. Yang. Diverse image-to-image translation via disentangled representations. In *Proceedings of the European conference on computer vision (ECCV)*, pages 35–51, 2018.
- [25] C. Li and M. Wand. Precomputed real-time texture synthesis with markovian generative adversarial networks. In *European conference on computer vision*, pages 702–716. Springer, 2016.
- [26] Z. Li and N. Snavely. Megadepth: Learning single-view depth prediction from internet photos. In *Proceedings of the IEEE Conference on Computer Vision and Pattern Recognition*, pages 2041–2050, 2018.
- [27] L. Liu, H. Jiang, P. He, W. Chen, X. Liu, J. Gao, and J. Han. On the variance of the adaptive learning rate and beyond. *arXiv preprint arXiv:1908.03265*, 2019.
- [28] J. Long, E. Shelhamer, and T. Darrell. Fully convolutional networks for semantic segmentation. In *Proceedings of the IEEE conference on computer vision and pattern recognition*, pages 3431–3440, 2015.
- [29] A. Mallya, D. Davis, and S. Lazebnik. Piggyback: Adapting a single network to multiple tasks by learning to mask weights. *arXiv preprint arXiv:1801.06519*, 2018.
- [30] A. Matsumoto and K. Yanai. Continual learning of image translation networks using task-dependent weight selection masks. In *Asian Conference on Pattern Recognition*, pages 129–142. Springer, 2019.
- [31] Y. A. Mejjati, C. Richardt, J. Tompkin, D. Cosker, and K. I. Kim. Unsupervised attention-guided image to image translation. *arXiv preprint arXiv:1806.02311*, 2018.
- [32] S. Mo, M. Cho, and J. Shin. Instagan: Instance-aware image-to-image translation. *arXiv preprint arXiv:1812.10889*, 2018.
- [33] M. Noroozi and P. Favaro. Unsupervised learning of visual representations by solving jigsaw puzzles. In *European Conference on Computer Vision*, pages 69–84. Springer, 2016.
- [34] J. Pennington, R. Socher, and C. D. Manning. Glove: Global vectors for word representation. In *Empirical Methods in Natural Language Processing (EMNLP)*, pages 1532–1543, 2014. URL <http://www.aclweb.org/anthology/D14-1162>.
- [35] M. Raghu, C. Zhang, J. Kleinberg, and S. Bengio. Transfusion: Understanding transfer learning for medical imaging. *arXiv preprint arXiv:1902.07208*, 2019.
- [36] M. Ravanelli, J. Zhong, S. Pascual, P. Swietojanski, J. Monteiro, J. Trmal, and Y. Bengio. Multi-task self-supervised learning for robust speech recognition. *arXiv preprint arXiv:2001.09239*, 2020.
- [37] V. Schmidt, A. Luccioni, S. K. Mukkavilli, N. Balasooriya, K. Sankaran, J. Chayes, and Y. Bengio. Visualizing the consequences of climate change using cycle-consistent adversarial networks. *arXiv preprint arXiv:1905.03709*, 2019.
- [38] V. Schmidt, M. Alghali, K. Sankaran, T. Yuan, and Y. Bengio. Modeling cloud reflectance fields using conditional generative adversarial networks. *arXiv preprint arXiv:2002.07579*, 2020.
- [39] A. Tarvainen and H. Valpola. Mean teachers are better role models: Weight-averaged consistency targets improve semi-supervised deep learning results. *arXiv preprint arXiv:1703.01780*, 2017.
- [40] P. Yanardag, I. Rahwan, M. G. Herranz, C. Fabian, Z. Rahwan, N. Obradovich, A. Dubey, and M. Cebrian. Can artificial intelligence induce empathy? deep empathy, 2017. URL <https://deepempathy.mit.edu/>.
- [41] R. Yi, Y.-J. Liu, Y.-K. Lai, and P. L. Rosin. APDrawingGAN: Generating artistic portrait drawings from face photos with hierarchical gans. In *IEEE Conference on Computer Vision and Pattern Recognition (CVPR '19)*, pages 10743–10752, 2019.
- [42] M. Zhai, L. Chen, F. Tung, J. He, M. Nawhal, and G. Mori. Lifelong gan: Continual learning for conditional image generation. In *Proceedings of the IEEE International Conference on Computer Vision*, pages 2759–2768, 2019.
- [43] J.-Y. Zhu, T. Park, P. Isola, and A. A. Efros. Unpaired image-to-image translation using cycle-consistent adversarial networks. In *The IEEE International Conference on Computer Vision (ICCV)*, Oct 2017.

## A. Implementation details

Our framework’s network architecture follows the baseline CycleGAN [43] with some differences in the generator to support self supervision. We use “ResnetBlock” to denote residual blocks [8]. “ $C \times H \times W$ -S-P Conv” represents a convolutional layer with  $C$  channels having kernel size



Model	Task	Start_Step	End_Step
LiSS	Rotation	0	24 000
	Jigsaw	24 000	158 000
	Depth	158 000	174 000
	Colorization	174 000	176 000
Sequential	Rotation	0	28 000
	Jigsaw	28 000	114 000
	Depth	114 000	122 000
	Colorization	122 000	124 000

Table 2: Transition steps for the flooded $\leftrightarrow$ non-flooded task. Translation starts when the colorization task is mastered.

$H \times W$  with padding  $P$  and stride  $S$ . “NConv” denotes a convolutional layer followed by an instance norm. “TConv” denotes transpose convolution layer proposed by Long et al. [28] followed by instance norm.

**Discriminator Network Architecture.** We use  $70 \times 70$  PatchGANs [15, 23, 25] as the one used in the original CycleGAN [43] baseline model shown in Table 3. The discriminator’s output is a real or fake label for overlapping  $70 \times 70$  patches. The GAN loss function then compares the target’s label real or fake to the average of patches predictions of the input image.

Table 3: Discriminator’s PatchGAN Architecture

Layer	Output	Activation
Input	$3 \times 256 \times 256$	None
$64 \times 4 \times 4 - 2 - 1$ Conv	$64 \times 128 \times 128$	LeakyReLU
$128 \times 4 \times 4 - 2 - 1$ NConv	$128 \times 64 \times 64$	LeakyReLU
$256 \times 4 \times 4 - 2 - 1$ NConv	$256 \times 32 \times 32$	LeakyReLU
$512 \times 4 \times 4 - 2 - 1$ NConv	$512 \times 31 \times 31$	LeakyReLU
$1 \times 4 \times 4 - 2 - 1$ Conv	$1 \times 30 \times 30$	None

**Encoder Network Architecture.** The encoder network’s architecture is inspired from [18], as shown in Table 4. The network starts with a reflection padding of size 3 and zero padded  $7 \times 7$  convolutions to avoid severe artifacts around the borders of the generated images, followed by  $3 \times 3$  convolutional blocks with padding 1 and stride 2 to downsample the input image and finally by 3 Residual Blocks.

**Translation and Colorization Head Architectures** The translation head’s network’s architecture follows the standard CycleGAN generator [43] as shown in Table 5. It consists of 3 residual blocks followed by upsampling convolutions. For colorization to share the encoder with other tasks, we repeat gray scale images along the channel dimension.

Table 4: Encoder’s Network Architecture

Layer	Output	Activation
Input	$3 \times 256 \times 256$	None
ReflectionPad $p=3$	$3 \times 262 \times 262$	None
$64 \times 7 \times 7 - 1 - 0$ NConv	$64 \times 256 \times 256$	ReLU
$128 \times 3 \times 3 - 2 - 1$ NConv	$128 \times 128 \times 128$	ReLU
$256 \times 3 \times 3 - 2 - 1$ NConv	$256 \times 64 \times 64$	ReLU
ResnetBlock	$256 \times 64 \times 64$	None
ResnetBlock	$256 \times 64 \times 64$	None
ResnetBlock	$256 \times 64 \times 64$	None

Table 5: Decoder and Colorization Network Architecture

Layer	Output	Activation
Input	$256 \times 64 \times 64$	None
ResnetBlock	$256 \times 64 \times 64$	None
ResnetBlock	$256 \times 64 \times 64$	None
ResnetBlock	$256 \times 64 \times 64$	None
$128 \times 3 \times 3 - 2 - 1$ TConv	$256 \times 128 \times 128$	ReLU
$64 \times 3 \times 3 - 2 - 1$ TConv	$64 \times 256 \times 256$	ReLU
ReflectionPad $p=3$	$64 \times 262 \times 262$	None
$3 \times 7 \times 7 - 1 - 0$ Conv	$3 \times 256 \times 246$	Tanh

**Rotation Network Architecture.** The rotation head’s architecture is inspired from [6] and shown in Table 6. The network performs a simple classification task out of 4 possible rotations ( $0^\circ$ ,  $90^\circ$ ,  $180^\circ$  and  $270^\circ$ ).

Table 6: Rotation Network Architecture

Layer	Output	Activation
Input	$256 \times 64 \times 64$	None
$256 \times 3 \times 3 - 2 - 1$ NConv	$3 \times 32 \times 32$	LeakyReLU
$256 \times 3 \times 3 - 2 - 1$ NConv	$3 \times 16 \times 16$	LeakyReLU
$2 \times 2$ MaxPool	$3 \times 8$	None
$128 \times 3 \times 3 - 2 - 1$ NConv	$3 \times 4 \times 4$	LeakyReLU
Flatten	2048	None
$2048 \times 4$ Linear	4	None

**Jigsaw Network Architecture.** Jigsaw’s network predicts the correct indices order of shuffled patches of an input image. The network consists of a set of convolutions extracting useful features from input image and then a fully connected layer to map it to the possible permutations. The model’s architecture shown in Table 7 performs a classification task over 64 possible permutations of shuffled images order.

**Depth Prediction Network Architecture.** Depth network architecture is inspired from [16] and shown in Table

Table 7: Jigsaw Network Architecture

Layer	Output	Activation
Input	$256 \times 64 \times 64$	None
$256 \times 3 \times 3 - 2 - 1$ NConv	$3 \times 32 \times 32$	LeakyReLU
$256 \times 3 \times 3 - 2 - 1$ NConv	$3 \times 16 \times 16$	LeakyReLU
$2 \times 2$ MaxPool	$3 \times 8$	None
$128 \times 3 \times 3 - 2 - 1$ NConv	$3 \times 4 \times 4$	LeakyReLU
Flatten	2048	None
$2048 \times 64$ Linear	64	None

8. The network is trained on labels predicted using a pre-trained MegaDepth Model [26].

Table 8: Depth Prediction’s Network Architecture

Layer	Output	Activation
Input	$256 \times 64 \times 64$	None
ResnetBlock	$256 \times 64 \times 64$	None
ResnetBlock	$256 \times 64 \times 64$	None
ResnetBlock	$256 \times 64 \times 64$	None
$128 \times 3 \times 3 - 2 - 1$ TConv	$256 \times 128 \times 128$	ReLU
$64 \times 3 \times 3 - 2 - 1$ TConv	$64 \times 256 \times 256$	ReLU
ReflectionPad p=3	$64 \times 262 \times 262$	None
$1 \times 7 \times 7 - 1 - 0$ Conv	$3 \times 256 \times 246$	None